Depression of Microphase-Separated Domain Size of Polyurethanes in Confined Geometry

Ken Kojio,[†] Yusuke Uchiba,[‡] Yoshitaka Mitsui,[‡] Mutsuhisa Furukawa,*[,‡] Sono Sasaki,[§] Hiroyasu Matsunaga,[§] and Hiroshi Okuda[⊥]

Department of Materials Science and Engineering, Faculty of Engineering, and Department of Materials Science, Graduate School of Science and Technology, Nagasaki University, 1-14 Bunkyo-machi, Nagasaki 852-8521, Japan; Japan Synchrotron Radiation Research Institute, 1-1-1, Koto, Sayo-cho, Sayo, Hyogo 679-5198, Japan; and International Innovation Center, Kyoto University, Kyotodaigaku Katsura, Saikyo-ku, Kyoto 615-8520, Japan

Received January 9, 2007
Revised Manuscript Received February 26, 2007

Introduction. For the past a decade, many researchers have been trying to clarify the chain structure and dynamics in the thin polymer films because they are not only of importance in the context of the basic physics of polymer chains but also have significant technological and practical impact.[1−8] Although these researches are still in controversy, these seem to be roughly divided into researches on "glassy" and "rubbery" polymers at room temperature by request of experimental limitation. First, on the glassy polymers, some groups claim that the T_g of ultrathin polystyrene considerably decrease in confined geometry. Second, T_g increased with decreasing film thickness for the rubbery polymers confined between solid substrates. That is, T_g can either increase or decrease as the film becomes thinner. For both cases, there are two obvious factors influencing the chain structure and dynamics of thin polymer films. One is the effect of surface and interface of polymer films. For example, the molecules around the interface are forced by interaction between films and substrate. The other one is the confinement effect. This induces changes in conformation and orientation of molecules due to reduction of space. Both factors become more obvious as the film thickness decreases. However, the fact relevant to these is not simple.

There are many ways to improve the structure and properties of multiphase polymer systems. Important methods are "blend" and "copolymerization" with two or more components. Furthermore, the copolymerization can be classified into random, graft, and block copolymerizations. One knows that the block copolymer exhibited the microphase-separated structure with the nanometer size because two different block sequences are chemically connected to each other, resulting in that each component cannot form large domains. Thus, the size of microphase-separated structure is controllable by change in the each block length. The structure itself as well as the size of microphase-separated domains can also be controlled by the ratio of two block sequences, incorporation of another component (triblock copolymer), and so on. Morkved et al. reported that the difference in the dielectric constants of the domains will force an orientation of the domains in the direction of the field lines for a multiphase system in which there is an anisotropy in the shapes of the phases, resulting in that the complete orientation of the morphology will result.[6] Also, it was revealed that the diblock microstructure orients normal to the surface by anchoring a random copolymer to the surface, which consists of monomer units identical to those of the block copolymer.[7] Improvement of the control of microstructure of copolymer is expected to give us an important technology.

From these backgrounds, we chose polyurethanes (PUs), which possess "strong polar groups in the molecular chains" and "$(AB)_n$-type multiblock structure". It is well-known that the polyurethanes consist of a hard segment and soft segment and exhibit microphase-separated structure. It is expected that the strong polar groups will help to form stable films even at the molecular level and strongly affect the microstructure of the polymer films. Also, the multiblock structure will restrict the segregation of lower surface free energy components at the film surface, resulting in the formation of the lateral phase separation. Here, we report the novel factor, "film thickness", as well as interfacial interaction for the controlling the size of microphase separation.

Methods. We synthesized PU with poly(oxytetramethylene) glycol (PTMG), 4,4′-diphenylmethane diisocyanate (MDI), and 1,4-butanediol (BD) by a prepolymer method. Two samples whose hard segment contents are 34 and 45 wt % were obtained for comparison (PU-34 and PU-45). The thin PU films were prepared onto a silicon wafer from the tetrahydrofuran PU solution by a spin-coating method. Then, the samples were dried under vacuum to remove residual solvent. Film thickness was controlled by changing solution concentration.

Fourier-tranform infrared (FT-IR) spectra were collected using a Biorad FTS-3000 equipped with a mercury−cadmium−telluride detector to investigate the molecular orientation in the PU films. For the transmission FT-IR measurement, double-side polished silicon wafer was employed. A p-polarized infrared beam was used, and incident angles were 10° and 74°.

XPS measurement was carried out to analyze the surface chemical composition of the PU films. PHI 5800 with monochromated X-ray source was employed. Emission angle employed were 75° and 30°, corresponding to analytical depths of 10.1 and 5.3 nm, respectively.

Microphase-separated structure of the PU films was observed using a Seiko Instrument AFM. Since the PU includes the rubbery soft segments at room temperature, we took an intermittent mode for the observation. Both topography and phase images were collected. To avoid the destruction of the sample surface, the images were acquired under ambient conditions using light to moderate tapping, $r = 0.90-0.80$, where $r =$ (set point amplitude/free amplitude of oscillation). Cantilevers employed were SI-DF-20 with spring constant of 14 N m^{-1} and resonance frequency of 130 kHz.

The interdomain spacing of microphase-separated structure in the PU films was investigated by grazing incident small-angle X-ray scattering (GISAXS) measurement. Measurements were carried out at the BL40 beamline in the Synchrotron radiation facility, SPring-8, Japan. Incident angle and exposure time were 0.15° and 60 s, respectively. In order to earn the sensitivity of the CCD camera, the beam stopper was placed along the azimuthal direction. Since the GISAXS patterns are obtained utilizing reflected X-ray beam, the scattered light, which comes from microphase-separated structure, is observed

* Corresponding author.
[†] Department of Materials Science and Engineering, Faculty of Engineering, Nagasaki University.
[‡] Department of Materials Science, Graduate School of Science and Technology, Nagasaki University.
[§] Japan Synchrotron Radiation Research Institute.
[⊥] Kyoto University.

10.1021/ma0700577 CCC: $37.00
Published on Web 03/15/2007

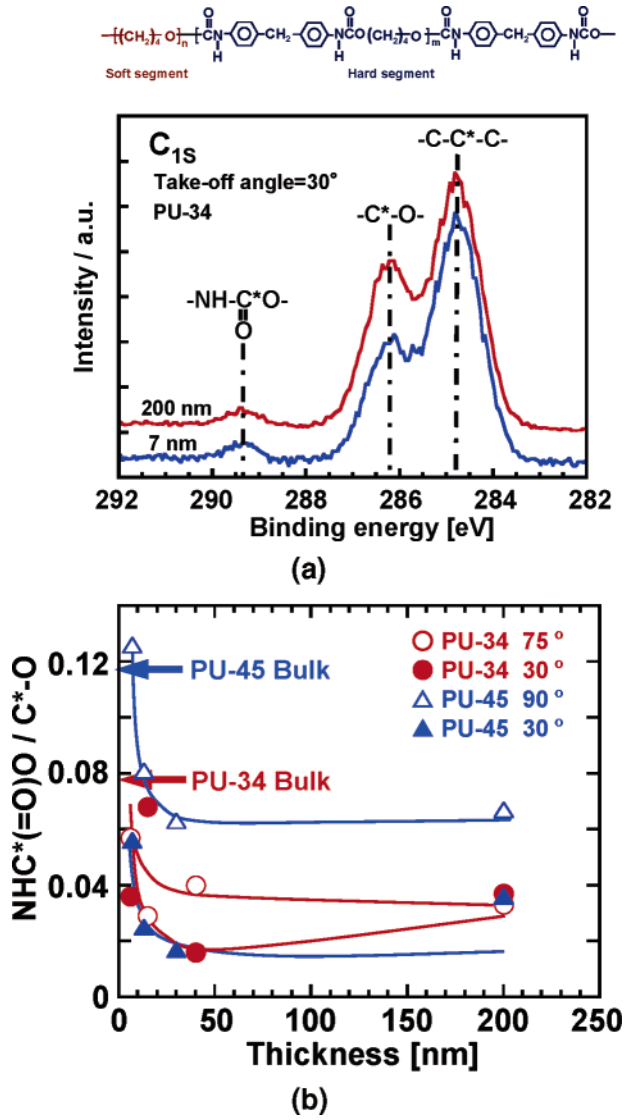

Figure 1. (a) XPS C_{1s} spectra for the thin PU films with 34 wt % of hard segment content (PU-34). The peaks observed at 284.8, 286.5, and 288.0 eV can be assigned to neutral carbon (CC*C), ether carbon (C*O), and urethane carbonyl carbon (NHC*(═O)O), respectively. As one can easily note, the peak intensity of NHC*(═O)O became larger than for C*O, indicating that the top layer was covered with lower surface free energy component, PTMG, for the thick film, and the hard segment domains have come out at the top surface at the smallest thickness. (b) The film thickness dependence of the intensity ratio of NHC*(═O)O to C*O (NHC*(═O)O/C*O). For the thin film, the ratio increased remarkably. This trend implies that "transition" occurred for the thinnest films.

on the Yoneda line. To discuss the peak position in the in-plane direction, intensity vs q profiles were obtained by integration along the Yoneda line. The interdomain spacing was simply decided using Bragg's equation. To decide the peak position of the GISAXS profiles, we subtract the baseline with silicon wafer from each profile and did peak fitting using the Gauss/Lorenz function.

Results and Discussion. First of all, we investigated surface chemical composition of the thin PU films using XPS. Figure 1a shows the XPS C_{1s} spectra for the thin PU-34 films with the thicknesses of 200 and 7 nm. The peaks observed at 284.8, 286.5, and 288.0 eV can be assigned to neutral carbon (C−C*−C), ether carbon (C*−O), and urethane carbonyl carbon (NH−C*(═O)−O), respectively. As one can easily note, the peak intensity of NH−C*(═O)−O and C*−O for the 7 nm thick film became larger and smaller than for the 200 nm one.

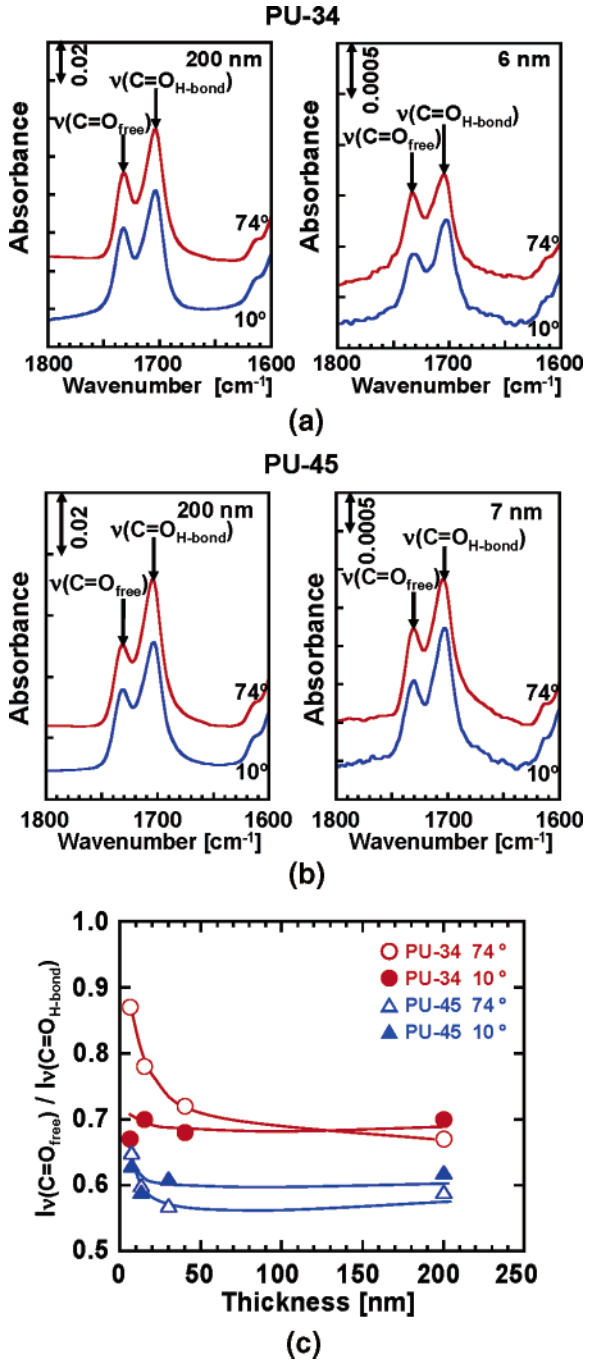

Figure 2. FT-IR spectra for the thin PU films with (a) 34 and (b) 45 wt % hard segment contents at incident angles of 10° and 74°. (c) Intensity ratio of (ν(C═O_{free}) peak to (ν(C═O_{H-bond}) one for both films. To evaluate the orientation of molecular chains in the PU films, p-polarized infrared beam and two different incident angles were employed. In the spectra shown here, one can see two peaks assigned to hydrogen-bonded carbonyl stretching band (ν(C═O_{H-bond})) and free one (ν(C═O_{free})). The intensity ratio of (ν(C═O_{free}) peak, to (ν(C═O_{H-bond}) exhibited larger magnitude for the film 6 nm thick at 74°. This indicates that the hard segment chains orient to the surface normal and/or the hard segment chains with free carbonyl groups oriented along the film/substrate interface with decreasing film thickness.

This result indicates that the lower surface free energy component, PTMG, was slightly enriched at the top surface for thick film. However, since the NH−C*(═O)−O peak was clearly observed for the thicker film even at an emission angle of 30°, the surface was not completely covered with PTMG layer at least at the 5 nm region. This is due mainly to the multiblock structure whose block sequence is smaller than 5 nm. In other

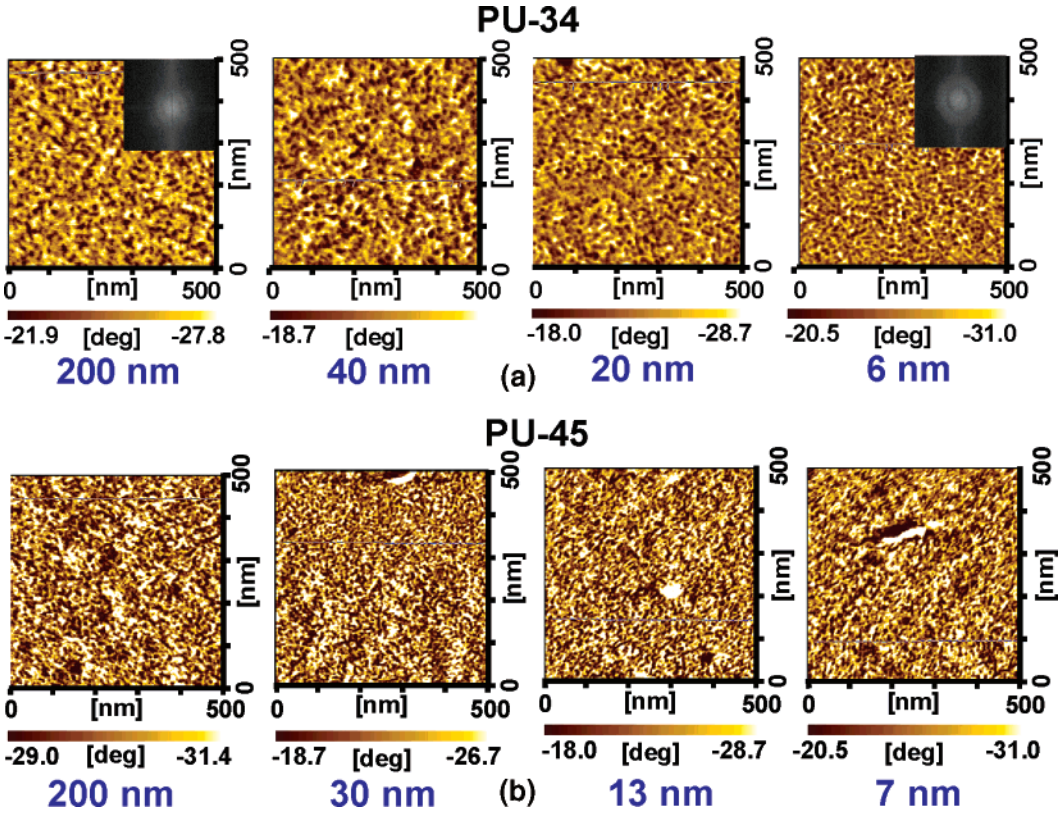

Figure 3. AFM phase images of the PU films with the hard segment content of (a) 34 and (b) 45 wt % at 200, 40, 20, and 6 nm thickness. For the 34 wt % films (PU-34 and PU 45 films), the interdomain spacing above 20 nm thickness was ca. 27 nm, whereas that was ca. 21 nm for the 6 nm thick film. On the contrary, the depression of interdomain spacing was observed at larger film thickness for the 45 wt % films. These results simply related to the relation between space and domain size.

words, the preferential surface segregation hardly occurs for the PU films. Figure 1b shows the film thickness dependence of the ratio of urethane carbonyl carbon to ether carbon (NH−C*(=O)−O/C*−O) for the thin PU films. The magnitudes of NH−C*(=O)−O/C*−O at 10 nm analytical depth (open symbols) were larger than for 5 nm analytical depth (filled symbols), indicating the PTMG was enriched at the top surface. The intriguing point here is that the magnitude dramatically increased with decreasing film thickness at around 10 nm thickness. These magnitudes of NH−C*(=O)−O/C*−O became close to those obtained for bulk. Since these results imply that the enrichment of the PTMG component at the top surface disappeared, the chain and/or microphase-separated structure may have changed below 10 nm thickness.

We investigated chain structure of the thin PU films using polarized FT-IR measurement. Figure 2 shows the FT-IR spectra for the thin PU films with hard segment contents of (a) the PU-34 and (b) PU-45 at incident angles of 10° and 74°. In the spectra shown here, one can see two peaks at 1704 and 1730 cm^{-1}. These peaks can be assigned to the hydrogen-bonded carbonyl stretching band ($\nu(C{=}O_{H-bond})$) and free one ($\nu(C{=}O_{free})$), respectively. The intensity ratio of the $\nu(C{=}O_{free})$ peak to $\nu(C{=}O_{H-bond})$ one ($I\nu(C{=}O_{free})/I\nu(C{=}O_{H-bond})$) of the PU-45 film is smaller than for the PU-34 one. This is due simply to the increasing the degree of microphase separation as the hard segment content increases. On the contrary, the magnitude of $I\nu(C{=}O_{free})/I\nu(C{=}O_{H-bond})$ for both films increased with decreasing film thickness at around 10 nm thickness. This roughly indicates the chain structure below 10 nm thickness is quite different from that of the thicker film. A detailed discussion on chain structure will be given later.

Next, we discuss the molecular orientation of the hard segment chains. $I\nu(C{=}O_{free})/I\nu(C{=}O_{H-bond})$ of both PU films at 74° exhibited larger magnitude in comparison with that at 10°. The electric field vector of incident infrared beam is almost perpendicular to the film surface at 74°, and the transition moment of the carbonyl stretching band is perpendicular to the molecular axis. Thus, FT-IR spectra give these two possibilities. One is that the hard segment chains with free carbonyl groups oriented to the parallel to the film/substrate interface with decreasing film thickness. The other one is that the hydrogen-bonded hard segment chains oriented to the surface normal. Anyway, dramatic change in chain structure occurred at the thinner film.

Figure 3 shows the AFM phase images of (a) the PU-34 and (b) PU-45 films with various film thicknesses. The brighter part corresponds to the larger phase lag region. It is quite hard to interpret the phase images because these images are formed by some factors, for example, surface elasticity, adhesion force, and so on. Concerning the occupied area, it seems reasonable to consider that the darker domains and brighter matrix correspond to the hard and soft segments, respectively. As one can see, the size of microphase-separated structure seems to be different depending on the film thickness; that is, the size of domains decreased with decreasing film thickness. For the PU-34 films, the size of microphase-separated domains was depressed at a thickness of 20 or 6 nm. The interdomain spacings of the PU-34 films were estimated to be 27 and 21 nm for 200 and 6 nm thicknesses, respectively, by fast Fourier transform (FFT) images. On the contrary, the same things happened for the PU-45 films. However, depression of domain size was observed at thicker thickness (30 nm) in comparison with the PU-34 film.

Figure 4 depicts that (a) the GISAXS pattern and (b) profiles for the PU-34 films with various thicknesses. Peaks assigned to interdomain spacing were clearly observed, and these peak

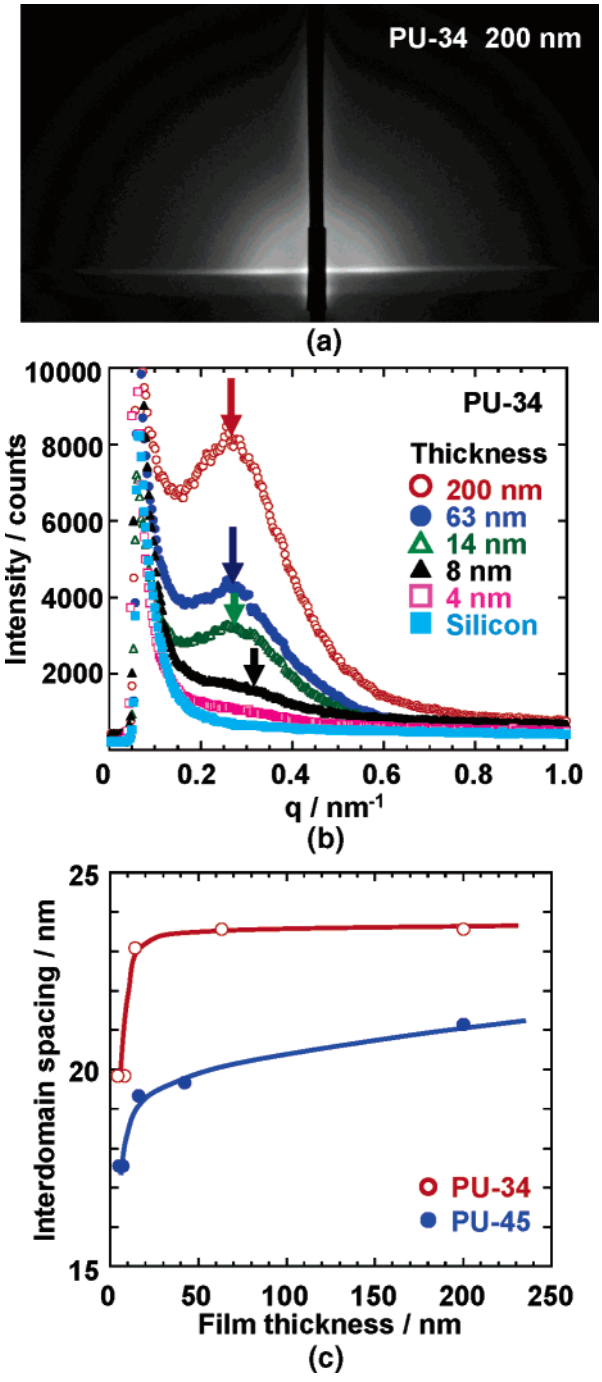

Figure 4. (a) GISAXS pattern for the PU film with 34 wt % (PU-34) at an incident angle of 0.15°. (b) GISAXS profiles for the PU-34 films. (c) Film thickness dependence of domain spacing for the PU-34 and PU-45 films. Note that the interdomain spacing abruptly decreased with decreasing film thickness for both films.

positions shifted to high q range with decreasing film thickness below 15 nm thickness, as shown in Figure 4b. Figure 4c shows film thickness dependence of interdomain spacing for the PU-34 and PU-45 films. The domain spacing abruptly decreased at around 10 nm thickness with decreasing film thickness. The domain spacings at 200 and 7 nm for the PU-34 were 24 and 20 nm, respectively. On the contrary, those for the PU-45 films continuously decreased with decreasing film thickness above 10 nm and then abruptly decreased. All these trends were almost the same as that obtained by AFM.

The reason that the size of microphase-separated domain decreases at thicker film thickness for the PU-45 films can be explained as follows. The occupied volume of the hard segment component for the PU-45 is greater than for the PU-34. The hard segment chains of the PU used in this study, −(MDI−BD)$_n$−, possess a high crystallizability.[9] Thus, the formation mechanism of the microphase-separated structure of the PU is deeply related to the crystallization of the hard segment chains. As the film thickness decreases, the space for the crystallization of the hard segment chains became smaller. That is, there is no enough space for the crystallization of the hard segment chains for the thinner films. Therefore, these depressions of domain size are thought to simply relate to the relation between space and domain size.

FT-IR measurement revealed that $I\nu(C{=}O_{free})/I\nu(C{=}O_{H-bond})$ increased with decreasing film thickness. We are now able to explain the reason. With decreasing film thickness, the size of the microphase-separated domains decrease as clarified by AFM and GISAXS, resulting in the amount of the interfacial region between hard segment domains and soft segment matrix increases. The degree of aggregation of the hard segment chains at the interface might be looser than for the hard segment domains. Thus, it seems reasonable to consider that the aggregation of the hard segment chains became weaker with decreasing film thickness as shown by FT-IR.

The size of microphase-separated domain decreases with decreasing film thickness. Although one can easily expect this simple phenomenon, there is actually no report. The most important reason that we could successfully attain is attributed to the "strong polarity" of the urethane groups. This leads to the strong interaction between the PU films and substrate surface, resulting in not only the formation of the stable thin films but also depression of the microphase-separated domain size for the first time.

Acknowledgment. This work was supported by the Asahi Glass Foundation, the Yazaki Memorial Foundation for Science and Technology, Japan Science and Technology Agency, Nagasaki Advanced Technology Development Council, and a Grant-in-Aid for Scientific Research (18750104) from the Ministry of Education, Culture, Science Sports and Technology of Japan.

References and Notes

(1) Maeda, N.; Chen, N.; Tirrell, M. T.; Israelachvili, J. N. *Science* **2002**, *297*, 379−382.
(2) Granick, S. *Science* **1991**, *253*, 1374−1379.
(3) Kajiyama, T.; Tanaka, K.; Takahara, A. *Macromolecules* **1997**, *30*, 280−285.
(4) Forrest, J. A.; Dalnoki-Veress, K.; Stevens, J. R.; Dutcher, J. R. *Phys. Rev. Lett.* **1996**, *77*, 2002−2005.
(5) Ge, S.; Pu, Y.; Zhang, W.; Rafailovich, M.; Sokolov, J.; Buenviaje, C.; Buckmaster, R.; Overney, R. M. *Phys. Rev. Lett.* **2000**, *85*, 2340−2343.
(6) Morkved, T. L.; Lu, M.; Urbas, A. M.; Urbas, E. E.; Ehrichs, E. E.; Jaeger, H. M.; Mansky, P.; Russell, T. P. *Science* **1996**, *273*, 931−933.
(7) Huang, E.; Rockford, L.; Russell, T. P.; Hawker, C. J. *Nature (London)* **1998**, *395*, 757−758.
(8) Tao, H.-J.; Meuse, C. W.; Yang, X.; MacKnight, W. J.; Hsu, S. L. *Macromolecules* **1994**, *27*, 7146−7151.
(9) Blackwell, J.; Lee, C. D. *J. Polym. Sci., Polym. Phys.* **1984**, *22*, 759−772.

MA0700577